Supplementary information

Bipyridine-containing π-conjugated polymers bearing optically active amide groups. Mechanistic aspects of formation of chiral higher-order structures

Taichi Sotani,[a] Mai Otoba,[a] Mio Hosotani,[a] Tomohiro Hayashi,[b] Hiromitsu Sogawa,[a] Fumio Sanda*[a]

[a] Department of Chemistry and Materials Engineering, Faculty of Chemistry, Materials and Bioengineering, Kansai University, 3-3-35 Yamate-cho, Suita, Osaka 564-8680, Japan

[b] Department of Materials Science and Engineering, School of Materials and Chemical Technology, Tokyo Institute of Technology, 4259 Nagatsuta-cho, Midori-ku, Yokohama, Kanagawa 226-8503, Japan

*Corresponding Author. E-mail: sanda@kansai-u.ac.jp.

Experimental Section

Measurements. ^{1}H (400 MHz), ^{13}C (100 MHz) NMR spectra were recorded on JEOL ECS-400 and ECZ-400 spectrometers. All NMR spectra were measured in $CDCl_3$. IR spectra were measured on a JASCO FT/IR-4100 spectrophotometer. Melting points (mp) were measured on a Yanaco micro melting points apparatus. ESI-TOF mass spectra were measured on a Shimadzu LCMS-IT-TOF. Number-average molecular weight (M_n) and polydispersity ($Đ$) values of polymers were determined by a size exclusion chromatography (SEC) system consisting of Shodex GPC KF-805L × 3, JASCO RI-4030, UV-4075, PU4180, CO-4060, AS-2055 Plus and LC-Net II/AD, using THF as an eluent at a flow rate of 1.0 mL/min, calibrated by polystyrene standards at 40 °C. CD and UV–vis spectra were recorded in a quartz cell (optical path length: 1cm) on a JASCO J-800 spectropolarimeter. Dynamic light scattering (DLS) measurements were performed using a square glass cell (PCS1115) on a Malvern Instruments Zetasizer Nano ZSP at 20 °C. The measured autocorrelation function was analyzed using a cumulant method, and the *Z*-average values were calculated from the Stokes-Einstein equations. Atomic force microscope (AFM) images were obtained using a commercial AFM system (MPF-3D, Oxford Instruments, UK). For the preparation of the sample for AFM, a silicon substrate was first cleaned by ultrasonication in acetone, then in ethanol, and finally in pure water (18.2 MW) (15 minutes in each solvent), followed by drying under nitrogen flow. Then, a drop of a solution of poly(**1**-**2**) in $CHCl_2CHCl_2$ (0.02 μM) was placed on the silicon substrate and dried under ambient conditions. The image in Figs. S14–S17 was obtained by fast force mapping using a sharp tetrahedral tip (tip radius < 10 nm, nominal spring constant = 0.2 N/m, ATEC-CONT, Nanosensors) at a scan size of 500 nm^2 with 256 × 256 scan points. Computational time was provided by the Supercomputer Systems, Academic Center for Computing and Media Studies, Kyoto University, and "Fugaku General Access Project"

(hp220357) from MEXT. Quantum mechanical calculations were performed with Gaussian 16,[S1] ES64L-G16 Rev B.01. The energies were calculated by the DFT method with the ωB97X-D functionals in conjunction with the basis sets, 6-31G* for C, H, N, O, and the semiempirical PM7 molecular orbital method. Molecular dynamics simulations were performed with GROMACS 2020.5,[S2] using the Universal Force Field[S3] modified by OBGMX.[S4] Solvent boxes for MD simulations were constructed using PACKMOL.[S5] The MD trajectories were analyzed using the GROMACS Analysis tools.

Materials. All solvents for the reaction were degassed by Ar bubbling and desiccated with molecular sieve 4A. All other reagents were commercially obtained and used as received without purification. L-Alanine dodecyl ester hydrochloride and 3,5-diethynyl benzoic acid were synthesized according to the literature.[S6,S7]

N-(3,5-Diethynylbenzoyl)-L-alanine dodecyl ester (1) EDC•HCl (5.34 g, 28.0 mmol) and DMAP (0.17 g, 1.40 mmol) were added to a solution of 3,5-diethynylbenzoic acid (2.36 g, 14.0 mmol) and L-alanine dodecyl ester hydrochloride (4.11 g, 14.0 mmol) in $CHCl_3$ (80 mL) and Et_3N (10 mL). The resulting solution was stirred at r.t. overnight. $CHCl_3$ (100 mL) was added to the mixture, and the mixture was washed with pure water. The organic layer was separated from the water layer, dried over $MgSO_4$, concentrated, and the residual mass was purified by silica gel column chromatography eluted with $CHCl_3/CH_3COOC_2H_5$ = 30/1 to obtain **1** as off-white solid (2.42 g, 3.63 mmol). Yield 26%. Mp 92 °C. ^{1}H NMR (400 MHz, $CDCl_3$): δ 0.88 (t, 3H, –CH_3, J = 6.9 Hz), 1.26–1.37 (m, 18H, –C_9H_{18}–), 1.53 (t, 3H, –CH_3, J = 7.5 Hz), 1.59 (s, 2H, –CH_2–), 3.15 (s, 2H, –C≡CH), 4.14–4.22 (m, 2H, –CH_2–), 4.73–4.80 (m, 1H, –CH<), 6.74 (d, 1H, –NH–, J = 7.3 Hz),

7.72 (t, 1H, Ar, J = 1.6 Hz), 7.84–7.88 (m, 2H, Ar) ppm. ^{13}C NMR (100 MHz, $CDCl_3$): δ14.2, 18.7, 22.8, 25.9, 28.6, 29.3, 29.4, 29.6 (2), 29.7, 32.0, 48.8, 66.0, 79.1, 81.7, 123.2, 130.9, 134.7, 138.3, 165.1, 173.2 ppm. IR (KBr): 3302, 3285, 3242, 2963, 2919, 2850, 2111 (C≡C), 1741 (ester C=O), 1632 (amide C=O), 1586 (N–H), 1541, 1356, 1309, 1200, 1155, 1121, 890, 678, 644 cm^{-1}. ESI-MS (m/z): $[M+H]^+$ calcd for $C_{26}H_{34}NO_3$, 410.2690; found 410.2698.

Scheme 1. Synthetic route of **1**.

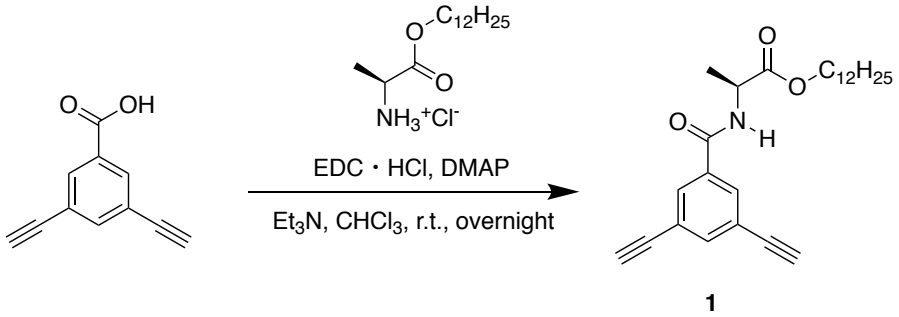

1

Polymerizations. All polymerizations were carried out in a Schlenk tube under Ar. Typical procedure: A solution of $PdCl_2(PPh_3)_2$ (35.1 mg, 0.005 mmol) and PPh_3 (13.1 mg, 0.005 mmol) in DMF (0.5 mL) and CuI (19.0 mg, 0.005 mmol) in Et_3N (0.1 mL) was added to a solution of **1** (205 mg, 0.500 mmol) and 4,4′-dibromo-2,2′-bipyridine (**2**, 157 mg, 0.500 mmol) in DMF (2.0 mL) and Et_3N (2.4 mL) under Ar, and the resulting solution was stirred at 80 °C for 18 h. The mixture was concentrated, and the residual mass was dissolved in $CHCl_2CHCl_2$ (10.0 mL). The resulting solution was poured into a large amount of MeOH to precipitate a solid mass. It was separated by filtration using a membrane filter (ADVANTEC H100A047A), washed with large amount of MeOH, and dried *in vacuo* to obtain poly(**1**-**2**) as greenish solid. Yield 72%.

Spectroscopic Data for the Polymers. Poly(**1**-**2**): ^{1}H NMR: (400 MHz, $CDCl_3$) δ 0.86–0.96 (m, 3H), 1.25 (m, 18H), 1.58–1.69 (m, 4H), 4.22 (br, 2H), 4.82 (br, 1H), 6.94 (br, 1H), 7.26–7.52 (br, 3H), 7.95 (br, 2H), 8.51–8.74 (br, 4H) ppm. IR (KBr): 3314, 3060, 2952, 2923, 2852, 2683, 2460, 2217, 1922, 1809, 1739 (ester C=O), 1650 (amide C=O), 1590 (N–H), 1567, 1533, 1457, 1392, 1354, 1202, 1166, 1100, 1053, 988, 890, 835 cm^{-1}. Poly(**1**-**3**): ^{1}H NMR: (400 MHz, $CDCl_3$) δ 0.86 (br, 3H), 1.10–1.40 (m, 18H), 1.40–1.80 (m, 4H), 4.18 (br, 2H), 4.81 (br, 1H), 6.82–7.00 (br, 2H), 7.42–7.61 (m, 7H), 7.76–7.88 (m, 3H), 7.94–7.99 (m, 2H) ppm. IR (KBr): 3339, 3060, 2974, 2928, 2877, 2853, 2802, 2755, 2738, 2677, 2600, 2571, 2527, 2491, 2352, 2236, 1739 (ester C=O), 1651 (amide C=O), 1591 (N–H), 1558, 1529, 1469, 1434, 1397, 1204, 1170, 1036, 890, 784, 691 cm^{-1}

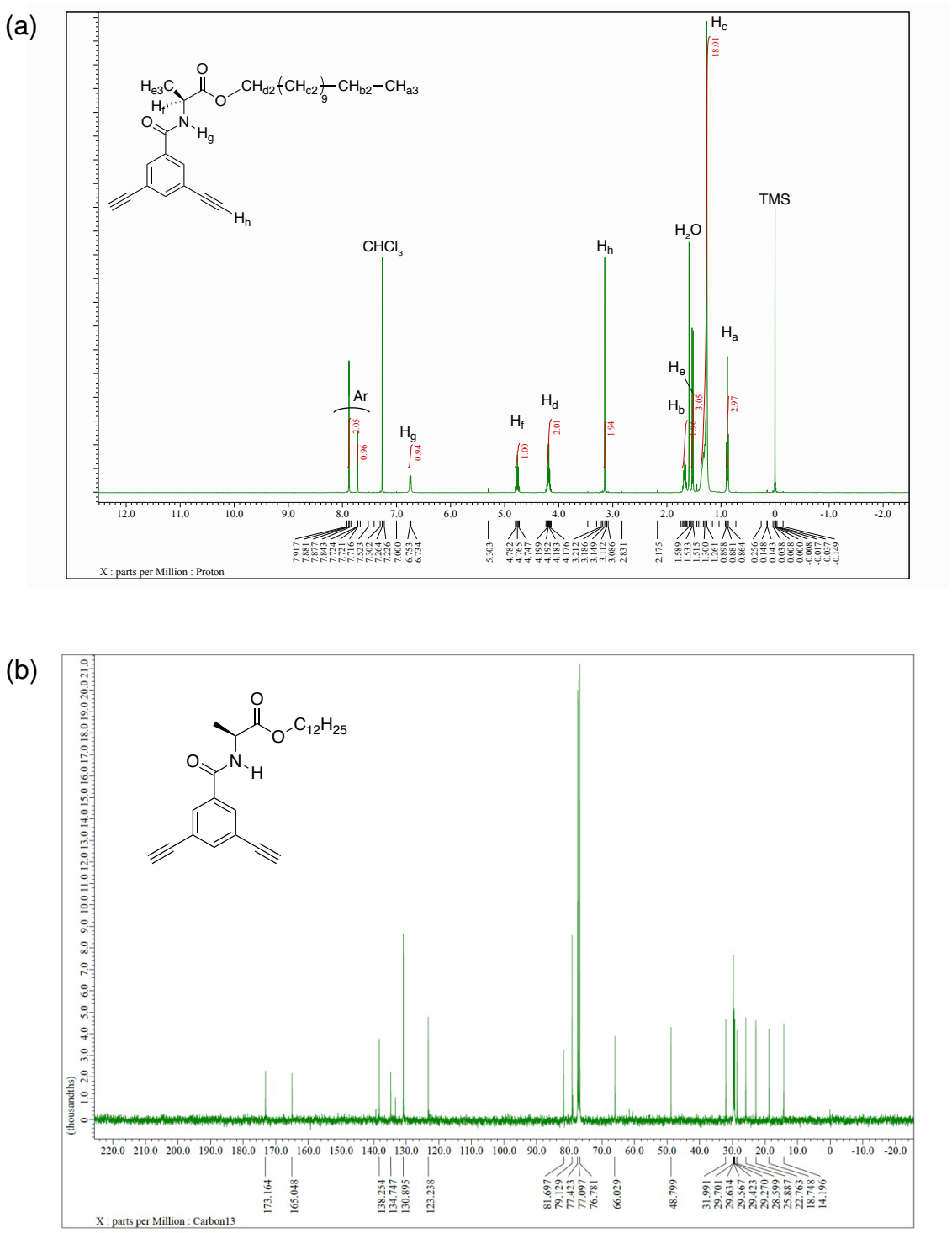

Fig. S1 (a) 1H (400 MHz) and (b) ^{13}C NMR (100 MHz) spectra of **1** measured in $CDCl_3$.

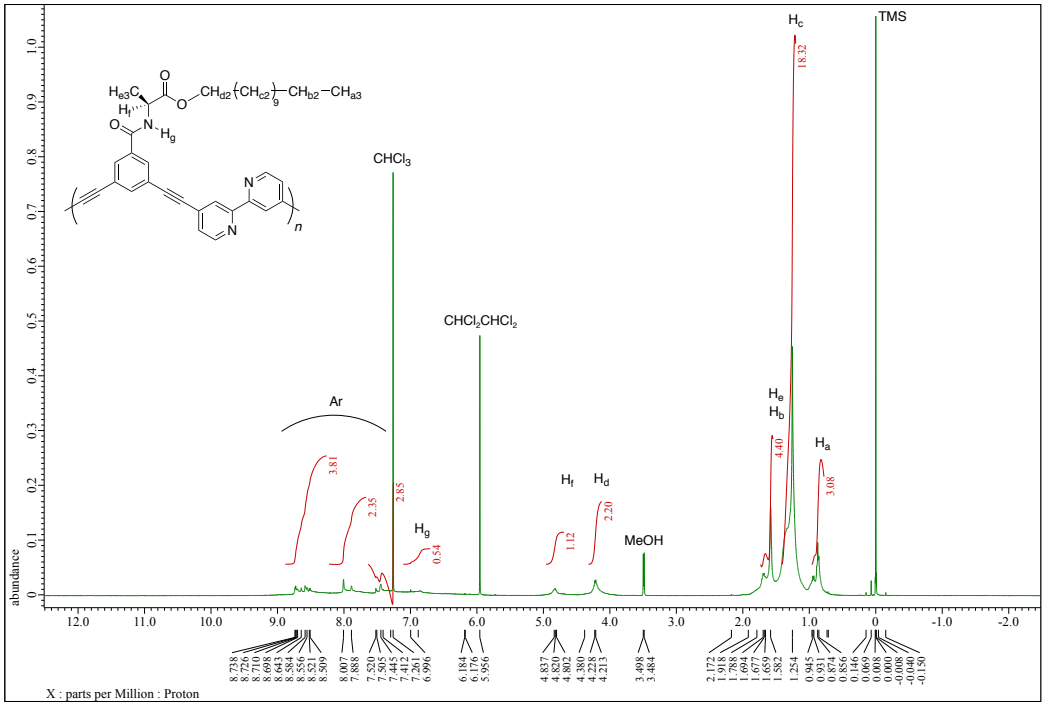

Fig. S2 ^{1}H NMR (400 MHz) spectrum of poly(**1**-**2**) measured in $CDCl_3$.

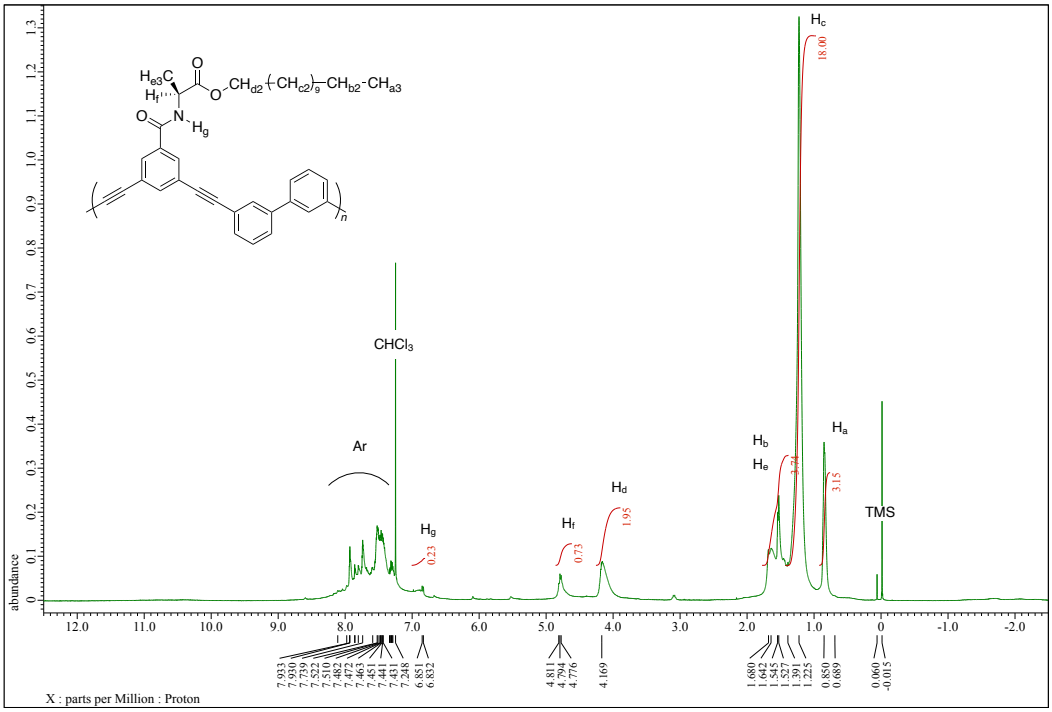

Fig. S3 ^{1}H NMR (400 MHz) spectrum of poly(**1**-**3**) measured in $CDCl_3$.

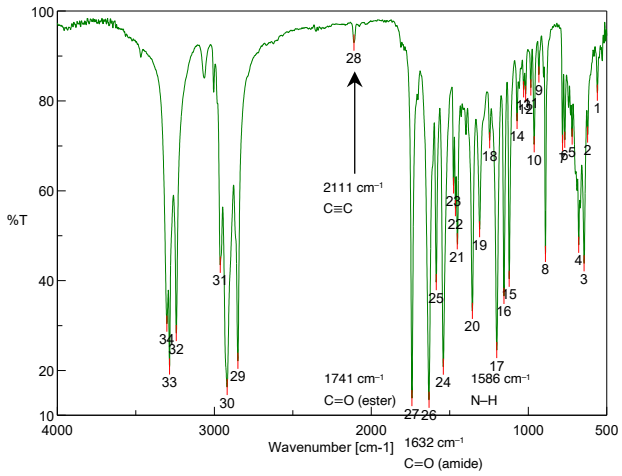

Fig. S4 IR absorption spectrum of **1** measured by KBr method.

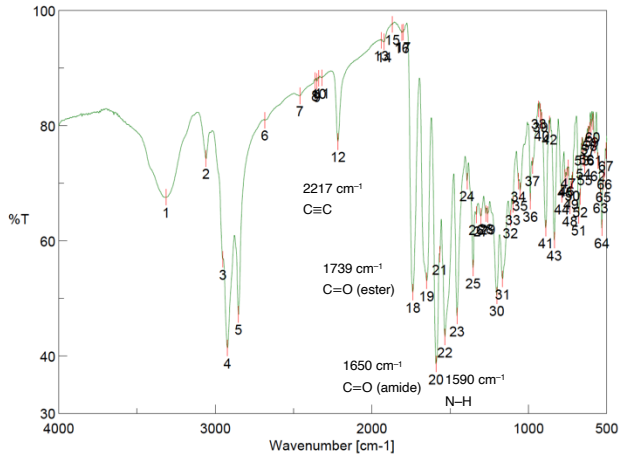

Fig. S5 IR absorption spectrum of poly(**1**-**2**) measured by KBr method.

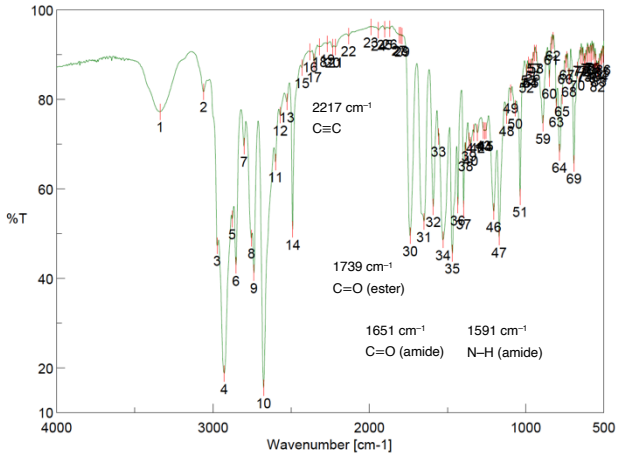

Fig. S6 IR absorption spectrum of poly(**1**-**3**) measured by KBr method.

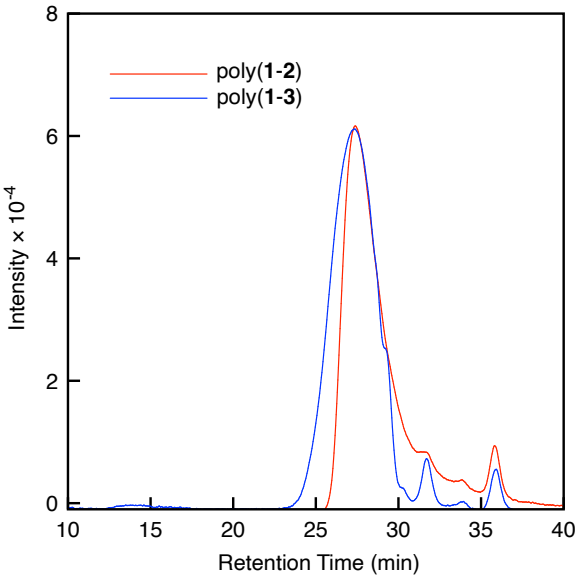

Fig. S7 SEC traces of poly(**1**-**2**) and poly(**1**-**3**) eluted with THF. The peak at 36 min is a ghost.

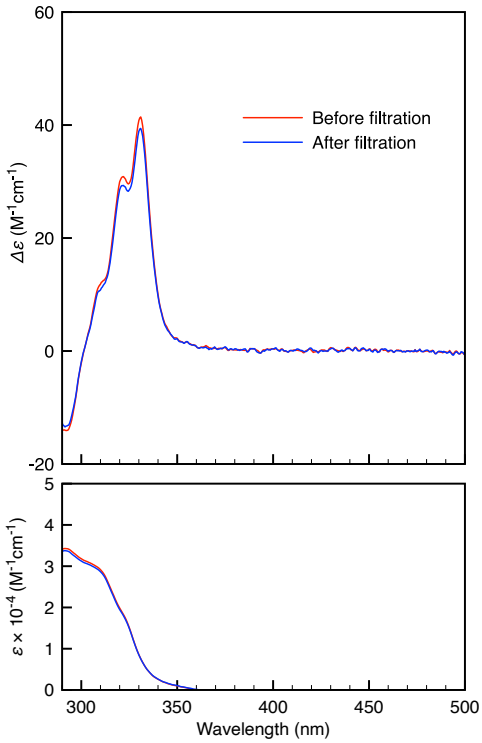

Fig. S8 CD and UV–vis absorption spectra of poly(**1**-**2**) measured in $CHCl_2CHCl_2$ (c = 0.02 mM) before and after filtration using a syringe filter (pore size = 200 nm) at 20 °C.

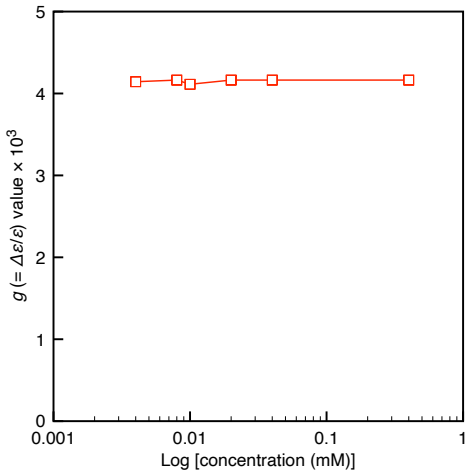

Fig. S9 Dependence of g (= $\Delta\varepsilon/\varepsilon$) values of poly(**1**-**2**) at 330 nm on concentration measured in $CHCl_2CHCl_2$ (c = 0.004–0.4 mM) at 20 °C.

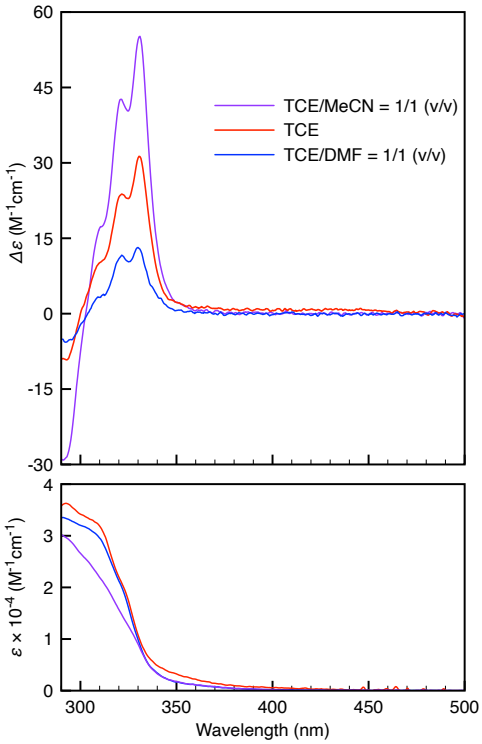

Fig. S10 CD and UV–vis absorption spectra of poly(**1**-**2**) measured in $CHCl_2CHCl_2/CH_3CN$ = 1/1 (v/v), $CHCl_2CHCl_2$ and $CHCl_2CHCl_2$/DMF = 1/1 (v/v) (c = 0.02 mM) at 20 °C, corresponding to Fig. 3.

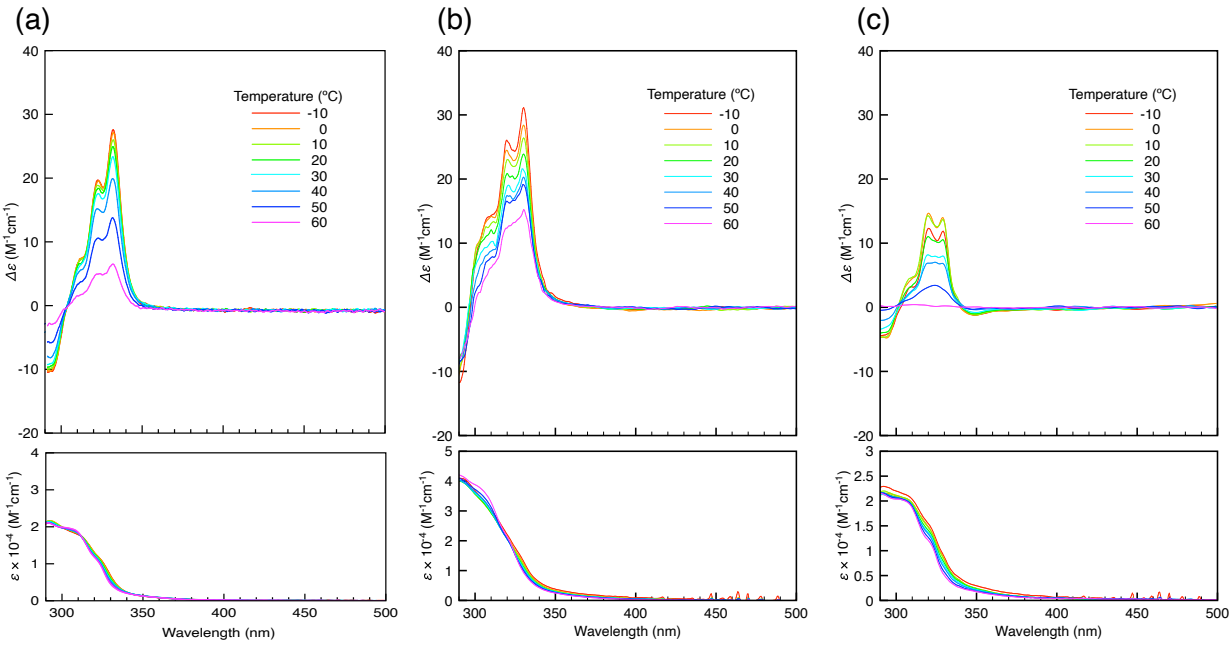

Fig. S11 Temperature-dependent CD and UV–vis absorption spectra of poly(**1**-**2**) measured in (a) $CHCl_2CHCl_2$, (b) $CHCl_2CHCl_2/CH_3CN$ = 1/1 (v/v) and (c) $CHCl_2CHCl_2$/DMF = 1/1 (v/v) (*c* = 0.02 mM).

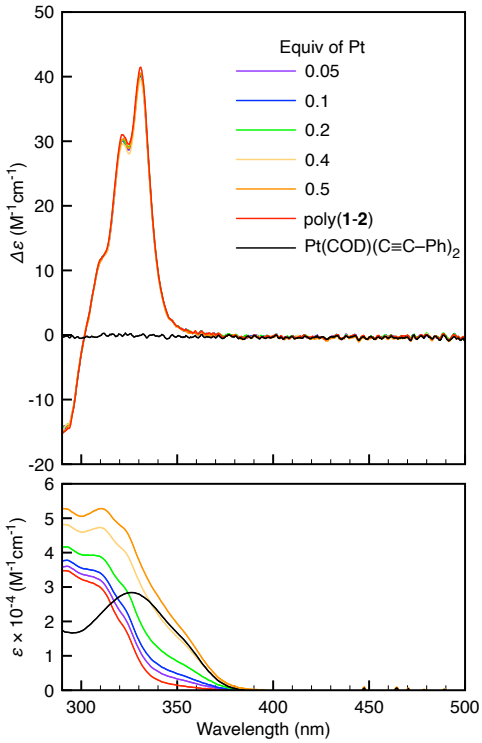

Fig. S12 CD and UV–vis absorption spectra of Pt(COD)(C≡C–Ph)$_2$ and poly(**1**-**2**) (c = 0.02 mM) with 0–0.5 equiv of Pt(COD)(C≡C–Ph)$_2$ in $CHCl_2CHCl_2$ at 20 °C.

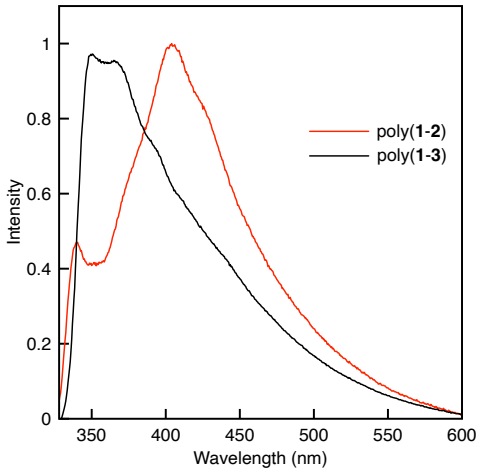

Fig. S13 Photoluminescence spectra of poly(**1**-**2**) and poly(**1**-**3**) excited at 308 nm measured in $CHCl_2CHCl_2$ (c = 0.04 mM).

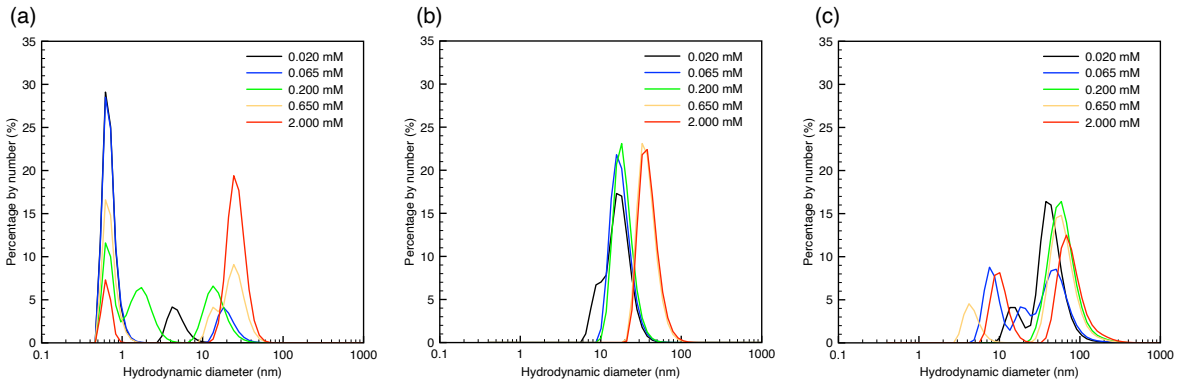

Fig. S14 Concentration-dependent DLS plots of poly(**1**-**2**) measured in (a) $CHCl_2CHCl_2$, (b) $CHCl_2CHCl_2/CH_3CN$ = 1/1 (v/v) and (c) $CHCl_2CHCl_2$/DMF = 1/1 (v/v) (c = 0.020–2.000 mM) at 20 °C.

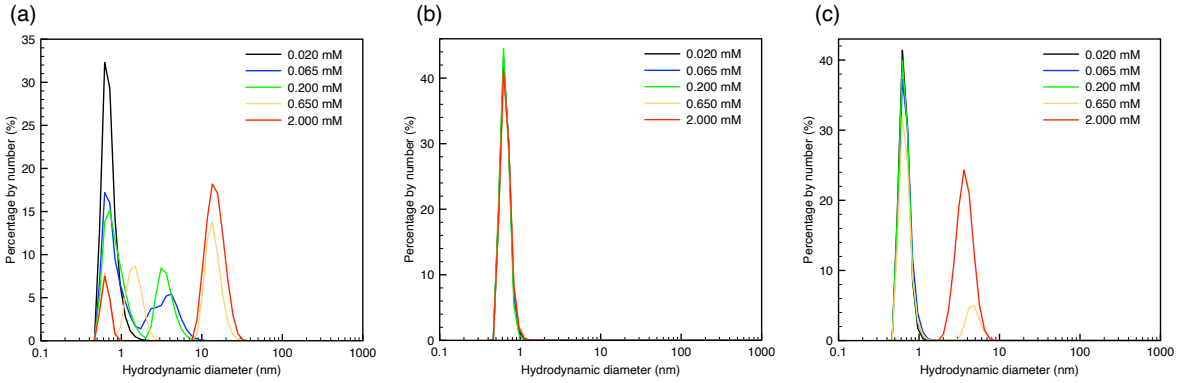

Fig. S15 Concentration-dependent DLS plots of poly(**1**-**3**) measured in (a) $CHCl_2CHCl_2$, (b) $CHCl_2CHCl_2/CH_3CN$ = 1/1 (v/v) and (c) $CHCl_2CHCl_2$/DMF = 1/1 (v/v) (c = 0.020–2.000 mM) at 20 °C.

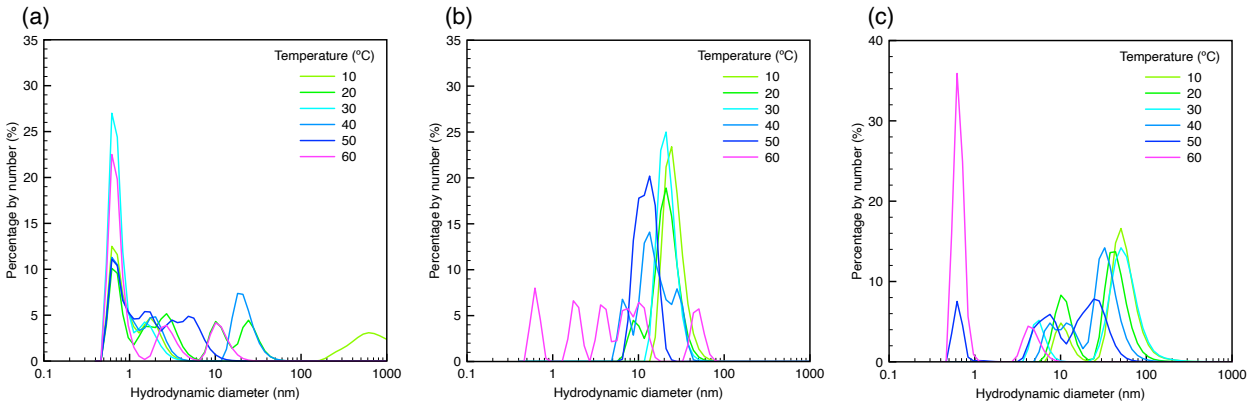

Fig. S16 Temperature-dependent DLS plots of poly(**1**-**2**) measured in (a) $CHCl_2CHCl_2$, (b) $CHCl_2CHCl_2/CH_3CN$ = 1/1 (v/v) and (c) $CHCl_2CHCl_2$/DMF = 1/1 (v/v) (c = 0.020 mM) at 10–60 °C.

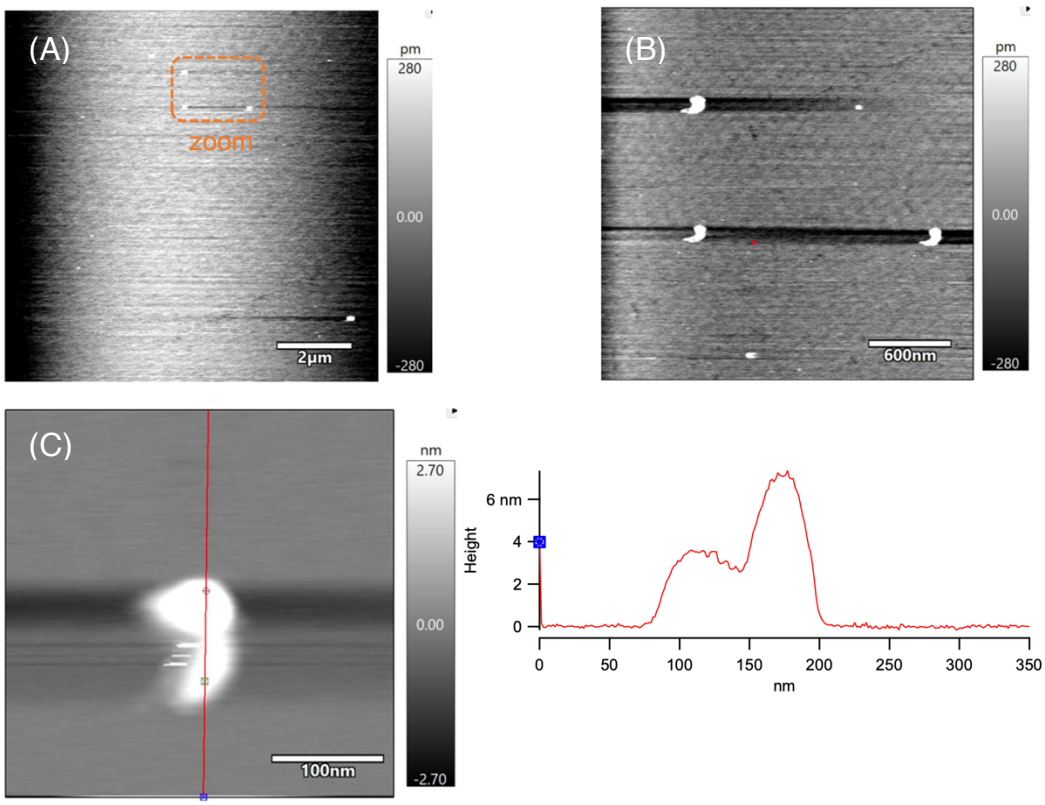

Fig. S17 (A) AFM images of poly(**1**-**2**). Force mapping by ATEC-cont. k = 0.3 N/m, resonance freq = 15 kHz, tip radius < 10 nm. Z-rate: 100 Hz, points & lines: 256×256 set point: 5.24 nN. Orange box = zoomed region 1. [Fig. S17 (B)]. (B) Zoomed region 1. Red box = zoomed region 2. [Fig. S17, (C)]. (C) Zoomed region 2.

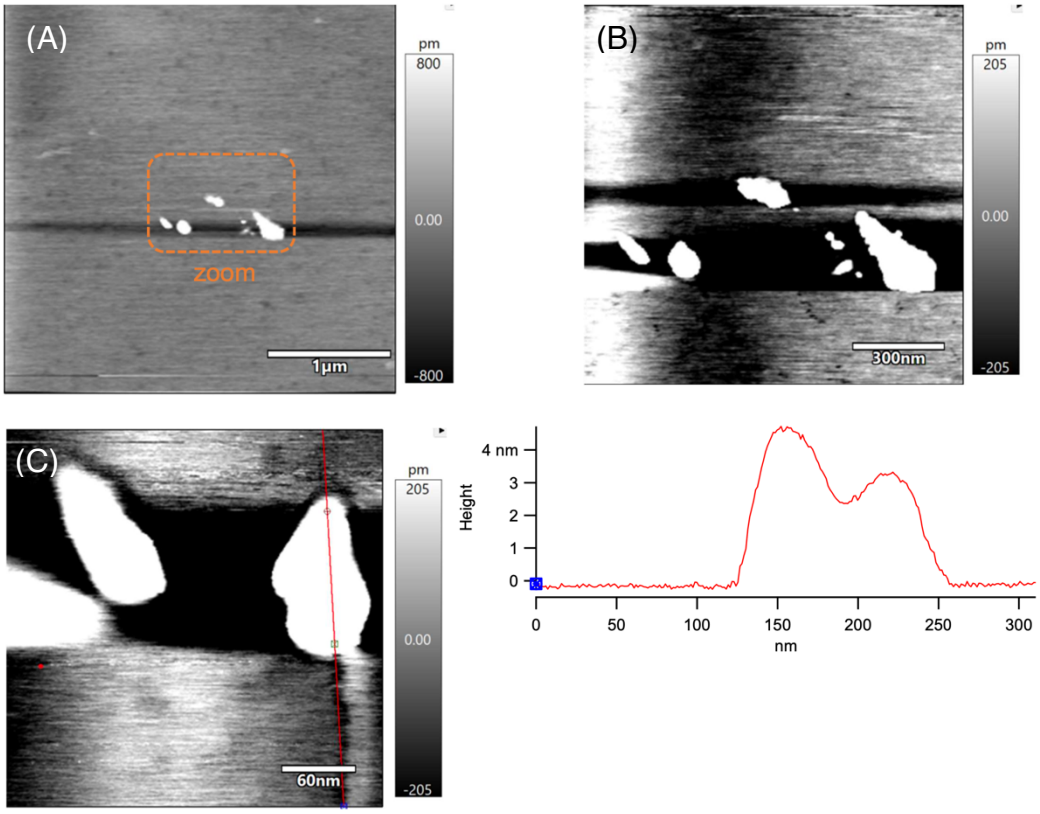

Fig. S18 (A) AFM images of poly(**1**-**2**). Force mapping by ATEC-cont. k = 0.3 N/m, resonance freq = 15 kHz, tip radius < 10 nm. Z-rate: 100 Hz, points & lines: 256×256 set point: 5.24 nN. Orange box = zoomed region 1. [Fig. S18 (B)]. (B) Zoomed region 1. Red box = zoomed region 2. [Fig. S18 (C)]. (C) Zoomed region 2.

References

S1) M. J. Frisch, G. W. Trucks, H. B. Schlegel, G. E. Scuseria, M. A. Robb, J. R. Cheeseman, G. Scalmani, V. Barone, G. A. Petersson, H. Nakatsuji, X. Li, M. Caricato, A. V. Marenich, J. Bloino, B. G. Janesko, R. Gomperts, B. Mennucci, H. P. Hratchian, J. V. Ortiz, A. F. Izmaylov, J. L. Sonnenberg, D. Williams-Young, F. Ding, F. Lipparini, F. Egidi, J. Goings, B. Peng, A. Petrone, T. Henderson, D. Ranasinghe, V. G. Zakrzewski, J. Gao, N. Rega, G. Zheng, W. Liang, M. Hada, M. Ehara, K. Toyota, R. Fukuda, J. Hasegawa, M. Ishida, T. Nakajima, Y. Honda, O. Kitao, H. Nakai, T. Vreven, K. Throssell, J. A. Montgomery, Jr., J. E. Peralta, F. Ogliaro, M. J. Bearpark, J. J. Heyd, E. N. Brothers, K. N. Kudin, V. N. Staroverov, T. A. Keith, R. Kobayashi, J. Normand, K. Raghavachari, A. P. Rendell, J. C. Burant, S. S. Iyengar, J. Tomasi, M. Cossi, J. M. Millam, M. Klene, C. Adamo, R. Cammi, J. W. Ochterski, R. L. Martin, K. Morokuma, O. Farkas, J. B. Foresman, D. J. Fox, Gaussian 16, Revision, B.01, Gaussian, Inc., Wallingford CT, 2016.

S2) M. J. Abraham, T. Murtola, R. Schulz, S. Páll, J. C. Smith, B. Hess and E. Lindahl, *SoftwareX*, 2015, **1–2**, 19–25.

S3) A. K. Rappé, C. J. Casewit, K. S. Colwell, W. A. Goddard III and W. M. Skiff, *J. Am. Chem. Soc.*, 1992, **114**, 10024–10035.

S4) G. Garberoglio, *J. Comput. Chem.*, 2012, **33**, 2204–2208.

S5) L. Martínez, R. Andrade, E. G. Birgin and J. M. Martínez, *J. Comput. Chem.*, 2009, **30**, 2157–2164.

S6) T. Sotani, T. Yajima, H. Sogawa and F. Sanda, *Macromolecules*, 2020, **53**, 11077–11088.

S7) H. Sogawa, Y. Miyagi, M. Shiotsuki and F. Sanda, *Macromolecules*, 2013, **46**, 8896–8904.